Toxicology Research

PAPER

View Article Online
View Journal | View Issue

Cite this: *Toxicol. Res.*, 2018, **7**, 1267

Neurotoxicity, behavioral changes and gene-expression profile of mice exposed to SnS_2 nanoflowers

Disi Bai,[a] Qingzhao Li,[b] Jianhui Wang,[b] Junjian Zhao,[c] Xuenan Deng,[b] Lu Yuan[b] and Ping Wu *[a]

Received 2nd August 2018,
Accepted 26th September 2018

DOI: 10.1039/c8tx00208h

rsc.li/toxicology-research

Recently, interest in the potential applications of tin disulphide nanoflowers (SnS_2 NFs) in the treatment of waste water and their antibacterial properties has increased. However, their effects on neurotoxicity, brain cognition and behavioural injury, as well as the underlying mechanisms of these effects have remained unknown. In the present study, we compared the neurotoxicity of SnS_2 NFs (50 nm) administered intragastrically at different doses (5, 10, and 50 mg kg^{-1}) in mice for 60 days. The results showed that the neurotoxicity of SnS_2 NFs in mice is dose-dependent. Furthermore, expression levels of genes related to oxidative stress, metabolism and signal transduction were also modified in the brain tissues of mice exposed to SnS_2 NFs, supporting the SnS_2 NF-dependent neurotoxic phenotype. Additionally, SnS_2 NF exposure resulted in an abnormal ultrastructure in the hippocampus of the treated mice. Nevertheless, their body weight, organ coefficient and behaviour assessed in an open-field test and learning and memory test results assessed using a Morris water maze test remained unaffected. This suggested that the increased risk of neurotoxicity in SnS_2 NF-treated mice was dependent on the dosage of SnS_2 NFs. The relative level of safety was <5 mg kg^{-1} for 50 nm SnS_2 NFs. The present study provides an experimental basis for the safe application of SnS_2 NFs; however, chronic behavioural effects of SnS_2 NFs remain unknown.

Introduction

Due to the novel physicochemical properties and functions of nanomaterials, they are highly attractive in various fields, such as industry, medicine, agriculture and food. Among the numerous types of nanomaterials, tin chalcogenide nanoparticles are semiconductors that have great potential applications, for example in solar cells,[1] holographic recording media, light-emitting diodes,[2] electrical switches,[3,4] lithium ion batteries,[5] gas sensors[6,7] and optical materials.[8] In recent years, in particular, there has been increasing interest in the use of semiconductors as photocatalysts to degrade organic contaminants.[9–11] Among the tin chalcogenides, tin disulphide (SnS_2) is an n-type semiconductor with a layered hexagonal structure and a larger band gap of 2.18–2.44 eV. Tin disulphide nanoparticles (SnS_2 NPs) are widely used in consumer products, including paints, textiles, and sunscreens and in the treatment of waste water. The photocatalytic application of SnS_2 has been considered in the degradation of the enrofloxacin antibiotic, which is part of the fluoroquinolone family.[12] Consequently, the risk of human exposure to SnS_2 NFs has increased, as the gastrointestinal tract becomes a key absorption route for SnS_2 NFs. Animal studies have suggested that neurological problems may occur due to exposure to nanomaterials,[13,14] implying that exposure to SnS_2 NFs may cause adverse health effects.

Some studies have reported that nanoscopic components of particulate matter can access the brain and could be associated with the onset of neurodegenerative diseases.[15,16] For example, nano-TiO_2 can easily cross the blood–brain barrier (BBB) and central nervous system (CNS) *via* the olfactory pathway or by oral administration, damaging brain neurons and resulting in neurodegenerative diseases and spatial recognition impairment.[17] We recently reported that an overdose of SnS_2 NFs by intraperitoneal injection could cause damage and increased permeability of the blood–testis barrier in mouse testicular tissue. In addition, nanoscopic SnS_2 particles exhibited greater reactivity than microscopic SnS_2 particles (200 nm). However, there was no significant difference

[a]*Department of Applied Physics, Institute of Advanced Materials Physics, Tianjin Key Laboratory of Low Dimensional Materials Physics and Preparing Technology, Faculty of Science, Tianjin University, Tianjin 300072, People's Republic of China. E-mail: pingwu@tju.edu.cn*
[b]*School of Public Health, North China University of science and technology, Bohai Avenue 21, Tangshan 063210, Hebei, People's Republic of China*
[c]*Clinical Lab, North China University of Science and Technology Affiliated Hospital, Jianshe Road 73, Tangshan 063000, Hebei, People's Republic of China*

between particles measuring 50 and 80 nm.[18] Furthermore, we also reported the hepatic effects of SnS_2 NFs on metabolic function and hepatotoxicity in mice, and we observed that increased risk of hepatotoxicity in SnS_2 NF-treated mice was independent of particle size but was dependent on dosage.[19] Therefore, in the present study, we chose 50 nm SnS_2 NFs to investigate their effects on neurotoxicity, brain cognition and behavioural injury, as well as the molecular mechanisms underlying these effects. Currently, it is unclear if SnS_2 NFs pose a hazard to human neurological health and their effects on the health of *in vivo* hippocampal neurons remain unknown. Therefore, the aim of this study was to investigate the toxicity of varying doses of SnS_2 NFs in mouse hippocampal neurons and to improve our understanding of the biological impact of SnS_2 NFs and its underlying mechanisms.

Materials and methods

Chemicals and characterization of SnS_2 NFs

The SnS_2 NFs (the diameter was 50 nm) with high purity were provided by the Department of Applied Physics, Tianjin Key Laboratory of Low Dimensional Materials Physics and Preparing Technology, Faculty of Science, Tianjin University.

SnS_2 NFs were synthesized by a one-step hydrothermal growth reaction. All the chemicals used in this experiment were of analytical grade without further purification. The method of synthesis and characterization of SnS_2 NFs has been introduced in our recent article.[18,19]

Pure $SnCl_4{\cdot}5H_2O$ was purchased from Tianjin Superstar st source Chemistry Technological Co., Ltd (Tianjin, China). Triton X-100 was purchased from Shanghai Yiteng Biological Science and Technology Co., Ltd (Shanghai, China). Pure ethanol amine was purchased from Shanghai Mindray Chemistry Technology Co., Ltd (Shanghai, China). Chemicals were all guaranteed reagents.

Animal rearing and treatment

As the main aim was to test whether SnS_2 NFs could induce neurotoxicity but not concerned about gender differences, male mice were employed in this study. Adult 40 specific-pathogen-free (SPF) CD-1 (ICR) male mice, body weight (BW) 29–33 g, were bought from the Laboratory Animal Center of North China University of Science and Technology. The mice were kept in plastic cages with a controlled environment at 22–26 °C, with 55–60% humidity and a 12 h light/dark cycle. Distilled water and sterilized food were available for mice *ad libitum*. Prior to dosing, the mice were acclimated to this environment for 5 days. This study was performed in strict accordance with the NIH guidelines for the care and use of laboratory animals (NIH Publication No. 85-23 Rev. 1985) and was approved by the Institutional Animal Care and Use Committee of National Tissue Engineering Center (Shanghai, China).

The doses investigated could conceivably be used in the degradation of pollutant bearing effluents, and thus could pose a hazard to human health. For the experiment, the mice were assigned randomly into 4 groups as follows: 3 groups of mice were treated with SnS_2 NFs (size: 50 nm, dose: 5, 10 and 50 mg per kg BW) by intragastric administration for 60 days (10 mice per group) for repeated-dose toxicity test. The control group was treated with deionized water without SnS_2 NFs, which was prepared by the same process to prepare SnS_2 NF suspension. The weight changes were monitored every week and general indexes variation was calculated.

Open-field test (OFT)

After 60 days, a 5 min open-field test was performed on each mouse. The open field apparatus was constructed of a wooden box and measured 60 × 60 cm with 60 cm walls. The entire apparatus was painted black except for the floor in white. The lines divided the floor into sixteen evenly spaced squares (15 × 15 cm). The central part consisted of 4 squares in the center of the apparatus. In the novel test situation, each animal was placed in the bottom right corner of the test apparatus and videotaped for 5 min using a video camera located 100 cm away from the arena. During each interval between the phases of experiments the arena was cleaned with cotton soaked in 70% alcohol. All videotapes were analyzed by the experimenter. For each mouse the following behaviors were recorded:

1. Locomotion: the number of lines crossed by the mouse over a 5 min interval

2. Rearing: the frequency of mice standing on their hind limbs

3. Self-grooming: rapid cleaning movements of the forelegs towards the face and/or the body. Both complete and non-complete grooming interrupted at some point along the body was counted together. (A typical complete grooming bout starts with the mouse scratching its face, progressively moving down along the body and terminating with the tip of the tail.)

4. Fecal pellets: the number of fecal pellets excreted by each individual mouse

5. Central latency: the time delay to enter the central part of the apparatus (*i.e.* the four squares in the center of the apparatus). An entry into the central part was scored when the mouse placed two front paws and the head in the respective area. Failure to enter the central part resulted in a latency score of 5 min for each measure.[20]

Morris water maze test

The Morris water maze was a circular pool (90 cm diameter and 30 cm height) filled with water (22 °C) to a depth of 14 cm and rendered opaque by the addition of small black balls. The pool was located in a dimly lit, soundproof test room with various visual cues, including a white-black colored poster on the wall, a halogen lamp, a camera and the experimenter. The maze was divided into four quadrants, and three equally spaced points served as starting positions around the edge of the pool. The order of the release positions varied systematically throughout the experiment. A circular escape platform (6 cm diameter and 12 cm high) was located in one

quadrant 1 cm above the water surface during the familiarization session and 1 cm below the water surface during the other sessions.

Video tracking was conducted with a video camera focused on the full diameter of the pool. Navigation parameters were analyzed by the Ethovision 3.1 video analysis system (Noldus, The Netherlands). The mice were trained in the Morris water maze five times daily (familiarization session, S1, S2, S3, S4). The following parameters were evaluated during each trial: escape latency (s) to find the hidden platform, the time spent in target quadrant (s), the mean distance to platform (cm) and the swim speed (cm s^{-1}). The escape latency, the time spent in the target quadrant and the distance to platform calculations were used as measures for the development of spatial memory whereas the swim speed was used to evaluate motor functions.

One familiarization and four acquisition sessions were performed using the Morris water maze. During the familiarization session and acquisition phase of the experiment, each mouse was given three trials. The delay between the trials was 60 s, and a 1 day interval was used between each session. For each trial, the mouse was taken from the home cage and placed into the water maze at one of three randomly determined locations with its head facing the center of the water maze. After the mouse had found and climbed onto the platform, the trial was stopped, and the escape latency was recorded. If the mouse did not climb onto the platform in 60 s, the trial was stopped, and the experimenter guided the mouse to the platform; the escape latency of 60 s was recorded.

Twenty-four hours after the last acquisition session, a 'probe trial' was used to assess the spatial memory retention of the location of the hidden platform. During this trial, the platform was removed from the maze and the mouse was allowed to search the pool for 60 s. The percent of time spent in each quadrant was recorded.[21]

Relative weight of the brain and preparation of hippocampus

After the OFT and Morris water maze test, all animals were sacrificed after being anesthetized with ether. The brains of all animals were quickly removed and placed on ice. After weighing the body and brain, the relative weight of the brain was calculated as the ratio of brain (wet weight, mg) to body weight (g), and the hippocampi were dissected and frozen at −80 °C.

The content of tin in whole blood and various parts of the body

Tissue samples including brain, liver, kidney, spleen, heart, testicle (each for 0.1 g) and 1.0 ml whole blood were taken from the SnS_2 NF-treated mice and control in each group, then digested, and analyzed for tin content. Inductively coupled plasma-mass spectrometry (ICP-MS, Thermo Elemental X7; Thermo Electron Co.) was used to analyze the tin concentrations in the samples. The working conditions of ICP-MS were as follows: emission power, 1420 w; frequency, 27.12; atomization pressure, 32Ibf/in2; auxiliary gas flow, 1.08 l min^{-1}; injection speed, 1.85 ml min^{-1}; dilute nitric acid (2%) flushing time, 1 min; ultrapure water flushing time, 1 min.

Histopathological examination of the brain

The fixed brain tissues were processed using standard laboratory procedures for histology.[22] Briefly, the tissues were embedded in paraffin blocks, deparaffinized in dimethylbenzene, hydrated in gradient ethanol and rinsed with distilled water, and sectioned perpendicular to the longest axis of the brain at a 4 μm thickness. The consecutive sections were stained with hematoxylin–eosin (HE) for light microscopic examination.

Observation of neuron ultrastructure

To observe ultrastructural modifications of the hippocampal neurons, brains were quickly removed from mice and placed on ice, and then the hippocampi were dissected. Hippocampi were fixed in a fresh solution of 0.1 M sodium cacodylate buffer containing 2.5% glutaraldehyde and 2% formaldehyde followed by a 2 h fixation period at 4 °C with 1% osmium tetroxide in 50 mM sodium cacodylate (pH 7.2–7.4). Staining was performed overnight with 0.5% aqueous uranyl acetate. The specimens were dehydrated in a graded series of ethanol (75, 85, 95, and 100%), and embedded in Epon812. Ultrathin sections were obtained, contrasted with uranyl acetate and lead citrate, and observed with a HITACHI H600 TEM (HITACHI Co., Japan).

Assay of oxidative stress

To evaluate the oxidative stress caused by SnS_2 NFs, brain samples were thawed, weighed and homogenized in 0.9% saline. The homogenates were centrifuged at 3000*g* at 4 °C for 10 min, and then the supernatant was harvested for biochemical assays. The superoxide ion ($O_2^{\bullet -}$) in the brain tissues was measured by monitoring the reduction in 2,3-bis (2-methoxy-4-nitro-5-sulfophenyl)-2*H*-tetrazolium-5-carboxanilide in the presence of $O_2^{\bullet -}$, as described by Oliveira.[23] The detection of H_2O_2 in the brain tissues was carried out by the xylenol orange assay.[24] Lipid peroxidation of the brain was measured using the commercial assay kit (Nanjing Jiancheng Bioengineering Institute, Jiangsu, China). MDA content was determined by measuring the levels of thiobarbituric acid reactive substances (TBARS) at 532 nm and expressed as nmol per milligram protein (nmol mg^{-1} prot).[25] Total protein concentration in brain homogenates was determined using the bicinchoninic acid (BCA) Protein Assay Kit (Boster Biological Technology, Wuhan, China). All the data were normalized to protein concentration. DNA of the brain was extracted using the DNeasy Tissue Mini Kit (Nanjing Jiancheng Bioengineering Institute, Jiangsu, China) as described by the manufacturer. Formation of 8-OHdG was determined using the 8-OHdG ELISA kit (Japan Institute for the Control of Aging, Haruoka, Japan). This kit provides a competitive immunoassay for quantitative measurement of the oxidative DNA adduct 8-OHdG. It was carefully performed according to manufacturer's instructions, and using a microplate varishaker-incubator, an automated microplate multireagent washer, and a computerized microplate reader.

RNA extraction and real-time qPCR

Total mRNA from brain tissues was extracted with the RNeasyplus mini kit (QIAGEN, Valencia, CA, USA) according to the manufacturer's instructions. The A260/280 ratio was found to be in the range of 1.8–2.0. The total RNA was converted into cDNA with 5 μg total RNA using Revert Aid First Strand cDNA Synthesis Kits (Fermentas, Hanover, MD, USA). Mouse-specific primers were designed and synthesized by Sangon Corp (Sangon Biotech Co., Ltd, Shanghai, China) (Table 1). To obtain the relative quantitative values for gene expression, the housekeeping gene β-actin was used as an internal control. Real-time PCR reactions were performed in an ABI PRISM 500 HT PCR system (Applied Biosystems, Framingham, MA, USA), and SYBR Green PCR Master Mix reagent kits (Roche Diagnostics, Shanghai, China) were used according to the manufacturer's instructions. The conditions for real-time PCR were as follows: 95 °C for 10 min followed by 40 cycles of 95 °C for 15 s, 60 °C for 1 min. After PCR, a melting curve analysis was performed to demonstrate the specificity of the PCR product. Every sample was analyzed in triplicate. The fluorescence threshold value was calculated using SDS2.2.1 system software and the $2^{-\Delta\Delta Ct}$ method was applied to quantitative calculation.[26]

Western blotting analysis

Expression of c-Fos, Cyp2e1, Dhcr7, NR1, NR2B, CaMKIV, and CREB1 was assayed by western blotting. Brain tissue extracts were obtained by homogenizing the sample in RIPA Buffer (Beyotime, Shanghai, China) supplemented with a protease inhibitor PMSF for 10 min. The homogenates were placed on ice for about 1 h and then centrifuged at10 000*g* for 10 min at 4 °C. The protein concentrations in the supernatant were determined using the BCA Protein Assay Kit (Boster Biological Technology, Wuhan, China). Each sample containing 50 μg protein was electrophoretically resolved on 8–10% SDS-polyacrylamide gels, and then transferred to polyvinylidine difluoride membranes (PVDF, Pall, Gelman Laboratory, USA). The membranes were first blocked with 5% non-fat milk in tris-buffered saline (TBS) containing 0.1% Tween-20 (TBST) for 1 h at RT and then incubated with specific primary antibodies: rabbit anti-c-Fos (1 : 1000, 26192-1-AP, Proteintech), rabbit anti-Cyp2e1 (1 : 1000, 19937-1-AP, Proteintech), rabbit anti-Dhcr7 (1 : 1000, 70-ab12888-400, MultiSciences), rabbit anti-NR1 (1 : 1000, 11404-1-AP, Proteintech), rabbit anti-NR2B (1 : 1000, 21920-1-AP, Proteintech), rabbit anti-CaMKIV (1 : 1000, 13263-1-AP, Proteintech), rabbit anti-CREB1 (1 : 1000, 12208-1-AP, Proteintech), and rabbit anti-β-actin (1 : 4000;

Table 1 List of primers used for real time RT-qPCR

Function	Gene name	Sequence (5′–3′)	Product length
Immediate early gene	c-Fos	F: GCTTTCCCCAAACTTCGACC R: GCGCAAAAGTCCTGTGTGTT	172
Oxidative stress	Cyp2e1	F: TGATGGCAAGCTGTACGTGT R: CACCGTGGAGTGATGGTGAA	76
	Dhcr7	F: TATGGGATGGGAGCCCGTTA R: GTACGAGGGGTCCTTAGGCT	159
Development	Xrn1	F: CAGTTTTCCCAAAGCTGCCC R: TCATCGGTCATCGTTCCCAC	88
Metabolism	NR1	F: CAGTGCCCCAGTGCTGTTAT R: CTCTCCCATCATTCCGTTCC	164
	NR2A	F: ATGAACCGCACTGACCCTAAG R: GGCTTGCTGCTGGATGGA	246
	NR2B	F: AATGTGGATTGGGAGGATAGG R: ATTAGTCGGGCTTTGAGGATACT	255
Signal transduction	CaMKIV	F: CAGAATAAAAGGTGCCACAGGC R: CGTCTCCGTGACGAAGTCAA	193
	CREB1	F: TCATCAGGCCCCTGACATTC R: CCAGGCCAGTTGTGATGACT	186
Neurotrophins	NGF	F: CAGATAGCAATGTCCCAGAAGG R: AGTGATGTTGCGGGTCTGC	149
	BDNF	F: GCCCAACGAAGAAAACCATAA R: ACACGCTCAGCTCCCCAC	188
Inflammation	Tnf-α	F: AGGGTCTGGGCCATAGAACT R: CCACCACGCTCTTCTGTCTAC	103
	Il-6	F: ACCAGAGGAAATTTTCAATAGG R: TGATGCACTTGCAGAAAACA	109
	Il-10	F: TGTCAAATTCATTCATGGCCT R: ATCGATTTCTCCCCTGTGAA	108
Apoptosis	Bax	F: GATCAGCTCGGGCACTTTAG R: TTGCTGATGGCAACTTCAAC	120
	Bcl-xl	F: GCTGCATTGTTCCCGTAGAG R: GTTGGATGGCCACCTATCTG	116
	Bcl-2	F: GGTCTTCAGAGACAGCCAGG R: GATCCAGGATAACGGAGGCT	113
	Bim	F: GCTCCTGTGCAATCCGTATC R: GCCCCTACCTCCCTACAGAC	116

Sungene Biotech, Tianjing, China) overnight at 4 °C, washed 3 times with TBST for 10 min and incubated with horseradish peroxidase-conjugated goat anti-rabbit IgG or goat anti-mouse IgG antibody (1 : 2000; Abgent, San Diego, CA, USA) for 1 h. The membranes were then developed by chemiluminescence using the Super Signal West Femto Chemiluminescent Substrate (ECL, Pierce Biotechnology Inc., Rockford, IL, USA) according to the manufacturer's instructions. Densitometric analysis was normalized using β-actin as the internal control. Quantity One software version 4.6.2 was used to quantify each band area and density in blots. Quantified band intensities are presented as fold of control. Three repeat experiments were performed independently.

Immunohistochemical staining

Immunohistochemical staining was performed with 5 μm paraffin cross-sections from the hippocampus. After deparaffinization with xylene they were rehydrated. Endogenous peroxidase activity was quenched with 3% hydrogen peroxide in methanol for 10 min, and then the slides were pre-incubated with 10% normal goat serum and then incubated with primary antibodies anti-NF-κB (14220-1-AP, Proteintech). Next, sections were washed in PBS, incubated with an appropriate biotinylated secondary antibody, washed and incubated with streptavidin–peroxidase. Staining was visualized by adding 3,3′-diaminobenzidine (DAB Substrate, Roche, Mannheim, Germany) with subsequent counterstaining using hematoxylin. Sections were rinsed in tap water, dehydrated through 70–100% graded alcohol, cleared in xylene and finally mounted in permanent mounting medium. Immunohistochemical micrographs were obtained with an FSX-100 microscope camera system (Olympus, Tokyo, Japan). Three sections were analyzed for each sample.

TUNEL assay

Hippocampus tissue processing for apoptosis-related DNA strand breaks analysis was also evaluated by terminal deoxynucleotidyl transferase dUTP nick end labeling (TUNEL) assay using the In situ Cell Death Detection kit, POD (Roche Diagnostics, Shanghai, China) according to the manufacturer's instructions. Briefly, 4 μm paraffin tissue sections were deparaffinized, hydrated and treated with proteinase K (Roche Diagnostics) for 15 min at 37 °C, in a humidifying chamber. The endogen peroxidase was blocked for 15 min in 3% H_2O_2 in methanol at room temperature (Roche Diagnostics). Thereafter, sections completely rinsed in PBS were incubated with the TUNEL reaction mixture (terminal deoxynucleotidyl transferase and labeled nucleotide mixture) for 60 min at 37 °C in a humidified atmosphere in the dark. After each step the tissue sections were rinsed twice, 5 min each. They were then incubated with converter-POD (anti-fluorescein conjugated with horse-radish peroxidase) for 30 min at 37 °C and counterstained with hematoxilin, dehydrated and mounted for light microscopy (Olympus, Japan). Cells containing the fragmented nuclear chromatin characteristic of apoptosis would exhibit a brown nuclear stain. Sections were viewed under a bright field at a magnification of ×400. The number of TUNEL-positive hippocampus cells was analyzed. Three sections were analyzed for each sample.

Statistical analysis

All data were presented as means ± standard deviation (S.D.) and analyzed using SPSS software version 12.0 (SPSS Inc., Chicago, Illinois). Differences between the control and the treatment groups were determined using a one-way analysis of variance (ANOVA) followed by the least significant difference (LSD) multiple range test. Three repeat experiments were carried out for each indicator studied. $P < 0.05$ was used as the criterion for statistical significance.

Results and discussion

Characterization of SnS_2 NFs

SnS_2 NFs have been characterized in our recent article.[18,19] Simply, SnS_2 NFs exhibit flowerlike structures with a diameter of 50 nm. Each flowerlike structure consists of tens of nanosheets, which act as building blocks. These nanosheets are connected to each other to build a 3D flowerlike structure. To investigate the disperse state of the 50 nm SnS_2 NFs in deionized water (DI H_2O) or phosphate-buffered saline (PBS), dynamic light scattering (DLS) and laser Doppler velocimetry (LDV) were performed to detect that. Table 2 shows agglomeration of the 50 nm SnS_2 NFs two times greater than their primary particle size at 116 nm in DI H_2O and four times nearly their primary size at 192 nm in PBS.[18]

To further understand how SnS_2 NFs behave and where it translocated across the digestive tract and then to the brain, the hydrodynamic sizes and zeta potential of SnS_2 NFs were examined using a Zetasizer (Malvern Nano-ZS90, Britain) to examine the aggregate or distributed status of SnS_2 NFs in acidic solution with Bovine Serum Albumin (BSA) or not at various pH values (Fed: stomach pH 2.98 and duodenum pH

Table 2 Characteristics of SnS_2 NFs in DI H_2O and phosphate buffered saline

Particle			LDV	
SnS_2 50 nm	Average diameter (nm)	PdI	Zeta potential (mV)	Electrophoretic mobility (μmcm V^{-1} s^{-1})
DI H_2O	116	0.385	−33.2	−2.59
Phosphate buffered saline	192	0.312	***	***

4.04; fasted: stomach pH 4.04 and duodenum pH 4.74 in mice). Table 3 shows agglomeration of the SnS_2 NFs (50 nm) at nearly 630 nm at pH 2.98, nearly 480 nm at pH 4.04, and nearly 380 nm at pH 4.74 without BSA. The agglomeration of the SnS_2 NFs (50 nm) at nearly 930 nm at pH 2.98, nearly 800 nm at pH 4.04, and nearly 750 nm at pH 4.74 with BSA is shown in Table 4. The results showed that the agglomeration of the SnS_2 NFs is increased in the same pH environment with BSA addition compared to that without BSA.

Body weight, relative weight of the brain, and tin accumulation in whole blood and brain tissues

In toxicological studies, changes in body weight and organ coefficient are two widely used, objective parameters. Specifically, brain coefficient is very important in assessing brain and nerve injury.[27] In the present study, the intragastric administration of 50 nm SnS_2 NFs at doses of 5, 10, and 50 mg kg^{-1} for 60 days did not produce significant changes in the net increase in body weight, brain coefficients, mental state, and food and water consumption ($P > 0.05$, Table 5).

In order to further study any neurological damage caused by SnS_2 NFs, the tin content was quantified and the ultrastructure was characterized in the hippocampus. Tin concentrations were significantly higher in the brain tissues of the middle- and high-dose SnS_2 NF treated groups ($P < 0.05$ and $P < 0.01$) than in controls, but there were no significant differences between high-dose and middle-dose groups ($P > 0.05$, Table 6). The results indicated that SnS_2 NFs can cross the blood–brain barrier to enter the brain tissue and accumulate in the hippocampus. And this was consistent with previous studies which reported that nanoparticle exposure could cause neurotoxicity in mice.[28–30]

Behavioral effects of SnS_2 NFs in the open-field test (OFT)

To examine the behavioral effects of SnS_2 NFs, we used the OFT as a well-established paradigm to measure locomotion, depression-like states, and anxiety-like behavior in animals. The OFT has been described as a suitable model for measuring levels of anxiety in animals, when they are confronted with a stressful or threatening situation.

As shown in Table 7, the SnS_2 NF groups did not differ in latency to enter the center compartment, the number of lines crossed, rearing, grooming, nor in the amount of defecation compared with the control group (ANOVA; $p > 0.05$). The results showed that exposure to SnS_2 NFs did not affect OFT behavior.

Effects of SnS_2 NFs on neurobehavioral profiles

To detect the ability of learning and memory of mice treated with SnS_2 NFs for 60 days, we used the Morris water maze (MWM) test in a dark and quiet environment. The results of

Table 3 Characteristics of SnS_2 NFs in solutions of different pH values without BSA

				LDV	
Particle	pH	Average diameter (nm)	PdI	Zeta potential (mV)	Electrophoretic mobility (μmcm V^{-1} s^{-1})
50 nm	2.98	614.7	0.322	−32.5	−2.74
	4.04	415.3	0.268	−31.1	−1.28
	4.74	375.9	0.473	−34.8	−2.19

Table 4 Characteristics of SnS_2 NFs in solutions of different pH values with BSA

				LDV	
Particle	pH	Average diameter (nm)	PdI	Zeta potential (mV)	Electrophoretic mobility (μmcm V^{-1} s^{-1})
50 nm	2.98	908.4	0.226	−35.2	−1.73
	4.04	812.9	0.413	−36.4	−1.52
	4.74	777.2	0.159	−32.8	−2.05

Table 5 Effects of different doses of SnS_2 NFs on the body weight increase and relative weight of the brain of mice

	SnS_2 NFs (50 nm)			
Index	0	5 mg kg^{-1}	10 mg kg^{-1}	50 mg kg^{-1}
Body weight increase (g)	17.53 ± 0.88	18.85 ± 0.81	18.22 ± 0.86	17.14 ± 0.75
Relative weight of the brain (mg g^{-1})	16.89 ± 0.72	16.33 ± 0.74	17.72 ± 0.66	15.92 ± 0.87

Mean ± S.D., *$P < 0.05$ *vs.* control group, **$P < 0.01$ *vs.* control group.

Table 6 Tin levels in each organ of ICR mice treated with different doses of SnS_2 NFs

	50 nm SnS_2 NFs (mg per kg BW)			
Indexes	0	5	10	50
Liver (μg g^{-1})	2.327 ± 0.075	2.472 ± 0.135	3.586 ± 0.247**	5.338 ± 0.497**
Kidney (μg g^{-1})	1.963 ± 0.134	2.218 ± 0.110	3.117 ± 0.305**	4.228 ± 0.272**
Spleen (μg g^{-1})	1.533 ± 0.207	1.805 ± 0.267	2.745 ± 0.152**	3.790 ± 0.212**
Testicle (μg g^{-1})	1.214 ± 0.088	1.286 ± 0.129	2.332 ± 0.263*	3.353 ± 0.183**
Brain (μg g^{-1})	0.981 ± 0.103	1.054 ± 0.151	1.883 ± 0.146**	2.206 ± 0.159**
Heart (μg g^{-1})	0.655 ± 0.126	0.861 ± 0.146	1.801 ± 0.224**	2.462 ± 0.244**
Blood (μg ml^{-1})	3.715 ± 0.152	4.093 ± 0.272	6.659 ± 0.319**	7.974 ± 0.565**

Mean ± S.D., *$P < 0.05$ *vs.* control group, **$P < 0.01$ *vs.* control group.

Table 7 Effects of different doses of SnS_2 NFs on the open field behavior in mice

Index	Latency to enter the center part (s)	No. of lines crossed	Rearing	Grooming	Fecal pellets
Control	39.30 ± 6.61	54.20 ± 6.94	8.10 ± 1.90	10.9 ± 1.72	1.80 ± 0.44
5 mg kg^{-1}	36.05 ± 4.66	63.30 ± 8.34	4.70 ± 1.18	9.30 ± 1.61	2.30 ± 0.56
10 mg kg^{-1}	31.91 ± 2.76	75.28 ± 8.92	7.50 ± 0.99	7.50 ± 0.99	1.50 ± 0.22
50 mg kg^{-1}	31.45 ± 3.80	52.04 ± 8.08	6.40 ± 1.34	9.90 ± 1.74	2.80 ± 1.22

the Morris water maze test are shown in Fig. 1. We first analyzed the swim speed in the first trial of the first session during the hidden platform training before mice from any of the four groups knew the location of the platform. There were no significant differences in the swim velocity among the groups (Fig. 1A). Subsequently, we used the escape latency to evaluate spatial learning and memory. No significant effects of experimental duration on the latency to locate the hidden platform were observed during the navigation in the MWM (Fig. 1B).

During the probe trial, the SnS_2 NF treated mice spent less time in the target quadrant when the platform was removed (Fig. 1C) and exhibited fewer platform crossings (Fig. 1D) but showed no significant difference compared with those of the control group.

Effects of SnS_2 NFs on oxidative damage and inflammation of the brain

There are large amounts of polyunsaturated fatty acids (PUFA) in the brain, which play an important role in the brain struc-

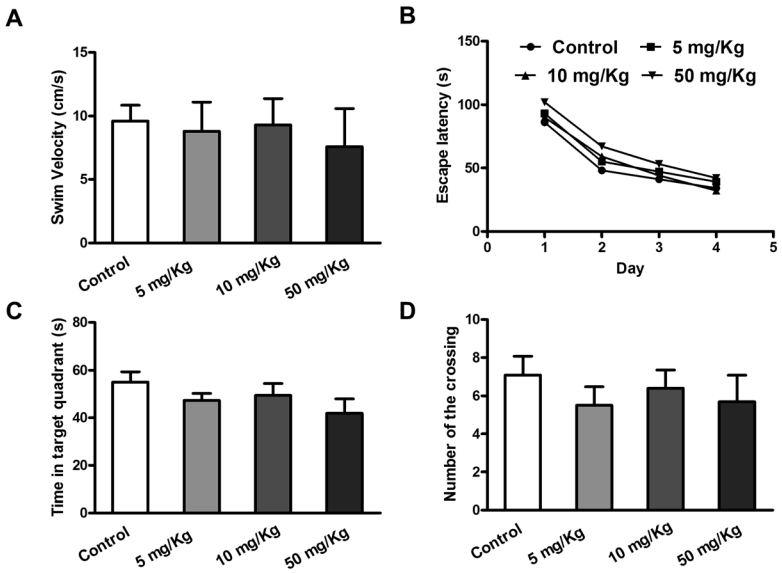

Fig. 1 SnS_2 NFs induced impairments of spatial learning and memory in MWM. (A). Swimming speed in the first trial of the first session during the hidden platform training. (B). Escape latency to reach the platform. (C). Time spent in the target quadrant in the probe trial. (D). Number of platform crossings in the probe trial. Bars represented mean ± S.D., $n = 10$.

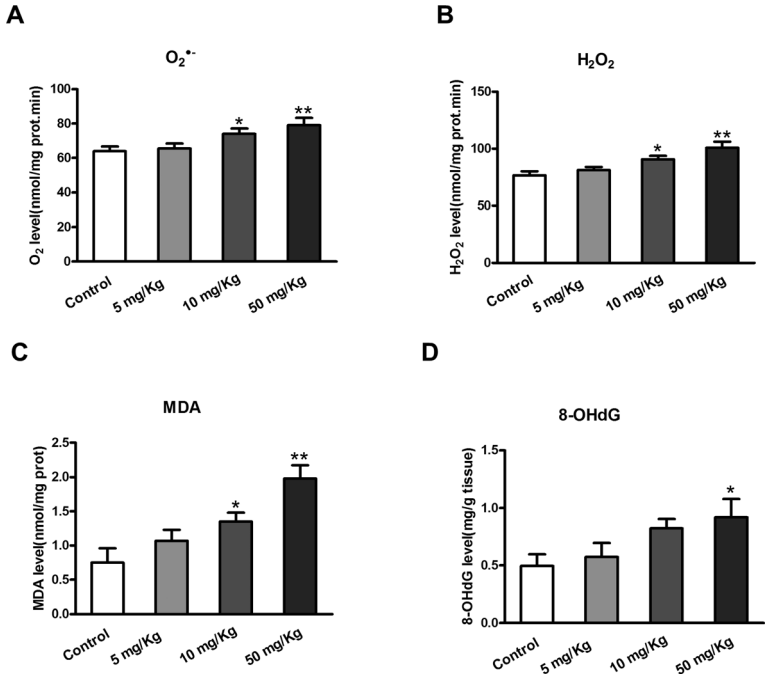

Fig. 2 The oxidative damage of the brain of ICR mice after intragastric administration with SnS_2 NFs for 60 consecutive days. Bars marked with a star are significantly different from the control (unexposed mice) at the 5% confidence level. Values represent mean ± S.D., n = 10.

ture and function. However, PUFA can be easily invaded by reactive oxygen species (ROS), which can impair cellular functions.[31] It can be seen from Fig. 2 that compared to the unexposed mice and the low dose group, the brains from the middle and high dose SnS_2 NF-treated mice exhibited greater vulnerability to oxidative stress, with significant increases in the generation rate of $O_2^{\bullet-}$ and H_2O_2, and higher levels of MDA and 8-OHdG as degradation products of lipid and DNA peroxidation ($p < 0.05$). Altogether, these results suggest that the brains of these SnS_2 NF-treated mice underwent oxidative stress.

Toxicity of nanoparticles is manifested by inflammation resulting from oxidative stress.[25,32–35] Tumor necrosis factor-alpha (TNF-α) and interleukin 6 (IL-6) are two pro-inflammatory factors. In contrast, interleukin 10 (IL-10) is a protective anti-inflammatory factor which will increase when inflammation or toxicity occurs.[36,37] In this study, the corresponding values in the 5, 10 mg kg^{-1} groups and controls were not significantly different, and the expression of TNF-α in the 50 mg kg^{-1} group was higher than in the control group ($P < 0.05$, Fig. 5A). Furthermore, weak immunohistochemical staining of NF-κB was seen in neuronal membranes in mice after treatment with 50 mg kg^{-1} SnS_2 NFs (Fig. 5B). This was consistent with the presence of inflammation as a consequence of NF-κB activation.

Effects of SnS_2 NFs on hippocampal histopathology and ultrastructure

Hippocampal pathology pictures are shown in Fig. 3A. For the control group, hippocampal cells with similar size arranged in neat rows could be observed (Fig. 3Aa). For the low dose-treated group, similar to the control, no signs of gross morphological changes were found in the hippocampus (Fig. 3Ab). As for the middle and high dose groups, the arrangement of hippocampal cells is not good anymore, while the cell contour is unclear and vacuolization could be seen. Furthermore, slight increases in the inter-cell distance and cell number, and a decrease in the cell volume are found (Fig. 3Ac-d). The results showed that middle and high dose SnS_2 NFs exposure has mild effects on hippocampal morphology in mice.

The changes in the hippocampal cell ultrastructure are shown in Fig. 3B. There were clear neuronal caryotheca, a large nucleolus and well-distributed chromatin in the hippocampus for the control group (Fig. 3Ba). However, with increasing SnS_2 NF dose, the cell ultrastructure in the SnS_2 NF-treated mice showed mild irregularity of the nuclear membrane (Fig. 3Bb-c); especially for the high dose group, shrinkage of the nucleus, chromatin marginalization, and mitochondrial swelling were found (Fig. 3Bd). These results demonstrated that the nanosize of SnS_2 is required for penetrating the blood–brain barrier and inducing hippocampus tissue injury.

Effects of SnS_2 NFs on immediate early gene, metabolism-related genes, signal transduction pathway genes and neurotrophins in the hippocampus

The expression of the immediate early gene c-Fos is an indirect marker of neuronal activity because c-Fos is often expressed when neurons are activated.[38,39] The upregulation of c-Fos mRNA in a neuron indicates recent activity.[40] First, we detected the expressions of early genes to determine whether

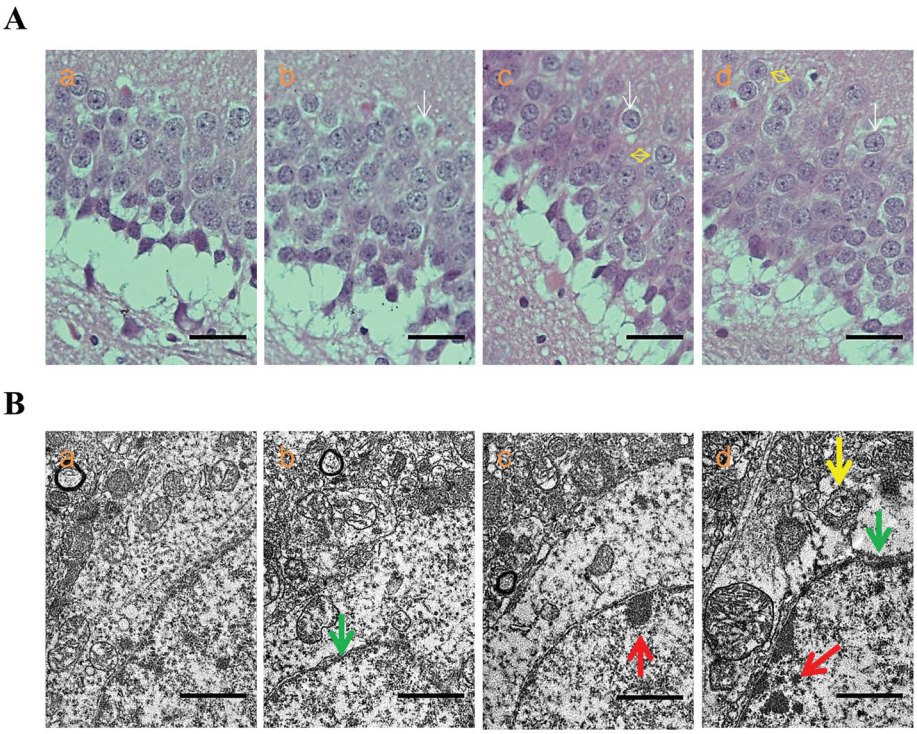

Fig. 3 Histopathological and ultrastructural changes in the brain of ICR mice caused by intragastric administration of SnS_2 NFs for 60 consecutive days. (A). Histopathological changes in the brain of ICR mice caused by intragastric administration of SnS_2 NFs. (a). Control. (b). 5 mg per kg BW SnS_2 NFs. (c). 10 mg per kg BW SnS_2 NFs. (d). 50 mg per kg BW SnS_2 NFs. White arrows indicate the vacuolization in hippocampal cells. The yellow double-headed arrow suggests the increased inter-cell distance. (B). Ultrastructural alterations of hippocampus cells of mice following SnS_2 NF exposure. Representative TEM micrographs were acquired from control (a) and SnS_2 NFs exposed mice (b–d) for 60 days, respectively. Green arrows indicate irregularity of the nuclear membrane, and significant shrinkage of the nucleus. Red arrows suggest chromatin marginalization. Yellow arrows exhibit mitochondria swelling.

any changes occurred in the hippocampus after SnS_2 NF exposure. The early gene c-Fos expression was significantly increased in the 10 and 50 mg kg^{-1} groups, compared with the control and 5 mg kg^{-1} groups (Fig. 4A, $p < 0.05$).

Recent studies showed that nanoparticles in mice affect the expression of genes for oxidative stress, immune response, apoptosis, memory and learning, development, signal transduction, metabolic process, DNA repair, response to stimuli, and cellular processes of the brain.[41–44] We therefore examined the effects of SnS_2 NFs on a panel of genes involved in oxidative stress, brain development, metabolism, signal transduction, and neurotrophins.[41,44]

In these experiments, 7 of the 11 genes showed significant differences correlating with SnS_2 NF-induced neurotoxicity. Among the genes encoding oxidative stress, Cyp2e1 increased and Dhcr7 decreased significantly in the high dose group (Fig. 4A, $p < 0.05$). Cytochrome P450 2E1 (abbreviated as Cyp2e1) is a member of the cytochrome P450 mixed-function oxidase system, which is involved in the metabolism of various endogenous substrates, such as steroids and fatty acids, and xenobiotics, including drugs, toxins, and carcinogens in the body.[45] According to the Cyp2e1-mediated oxidative stress pathway, it seems reasonable to conjecture that exogenous Cyp2e1 inducers such as ethanol, acetone, and SnS_2 NFs could cause overexpression of Cyp2e1, which further promoted the use of H^+ from reduced nicotinamide adenine dinucleotide phosphate and H_2O and produced nicotinamide adenine dinucleotide phosphate and $O_2^{\bullet-}$, resulting in peroxidation and pathologic changes in SnS_2 NF-exposed mice. 7-Dehydrocholesterol reductase (Dhcr7) plays a role in drug-induced malformations and inhibits cholesterol biosynthesis, which severely impair brain development.[46] In this study, the mRNA expression of Dhcr7 was significantly decreased compared to the control group (Fig. 4A, $p < 0.05$), suggesting the weakening ability of the brain removing free radicals and aggravating the lipid peroxidation situation (Fig. 2). This result was consistent with the results of the oxidative stress assay.

The hippocampus is essential for learning and memory. Synaptic transmission and plasticity in the hippocampus are mediated by *N*-methyl-D-aspartate (NMDA) glutamate receptors.[47,48] When investigating the expression of NMDA and genes involved in its signal transduction pathway, we found that the expression levels of NMDA receptor genes such as NR1 and NR2B were significantly upregulated in the hippocampus of mice exposed to SnS_2 NFs. The expression of NR1 mRNA was significantly higher in the 10 mg kg^{-1} group than in the control and other SnS_2 NF-treated groups, the expression of NR2B mRNA was significantly higher in the 10

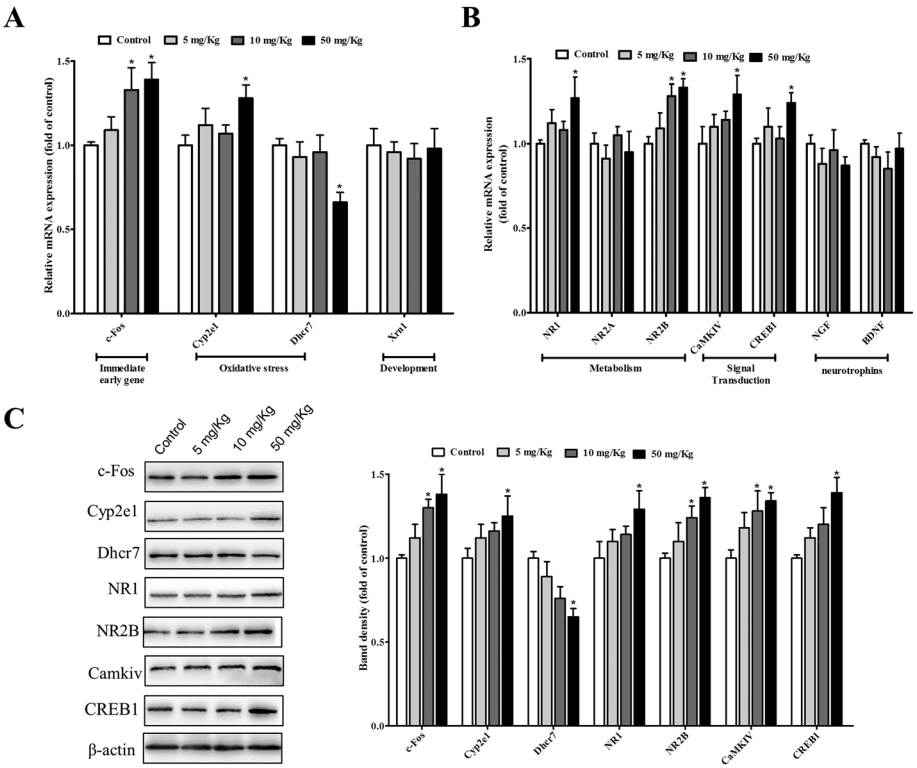

Fig. 4 Transcription levels of mRNAs encoding immediate early gene, oxidative stress, development, metabolism, signal transduction, and neurotrophins relative genes in brain tissues of mice following SnS_2 NF exposure. (A) Immediate early gene c-Fos, oxidative stress, development relative gene expressions in the hippocampi of controls and SnS_2 NF exposed mice. (B) NMDA receptor subunits: NR1, NR2A, and NR2B; transcription factor: CaMKIV, CREB1; neurotrophins: NGF, BDNF in the hippocampi of controls and SnS_2 NF exposed mice. Each bar represents the mean ± S.D. (n = 10, * $p < 0.05$). (C) The protein levels of the relative genes that have changes in mRNA levels by western-blot analysis. β-Actin was used as the internal control. *$P < 0.05$ *vs.* control.

and 50 mg kg^{-1} groups than in the other groups, while the expression of the NR2A mRNA did not differ among the four treated groups (Fig. 4B, $p < 0.05$). Glutamate is a ligand for the NMDA receptor and an excitatory amino acid neurotransmitter and one of the neurotoxic markers in the brain. The imbalance of Glu metabolism triggered up-regulations of NMDA subunit (such as NR1 and NR2A) expression in the hippocampus. We can speculate that SnS_2 NFs may induce the release of glutamate from neurons and the release of toxic substances, such as inflammatory mediators, and oxidative stress from microglia, possibly triggering neuroinflammation and/or cognitive impairment. Multiple protein kinases have been demonstrated to translocate to the nucleus to activate the transcriptional activator CREB in NGF signal transduction pathways. We assayed the gene expression of CaMKIV, which phosphorylates CREB, and observed significant reductions in CaMKIV expression in the high dose SnS_2 NF-exposed hippocampus of mice (Fig. 4B, $p < 0.05$). We also examined the expression of NGF-related transcriptional factor, CREB1 expression in the hippocampus, suggesting marked up-regulation of the gene expression of CREB1 due to the high dose SnS_2 NF exposure (Fig. 4B, $p < 0.05$). However, the expressions of neurotrophins, such as NGF and BDNF, did not differ between the control and other groups (Fig. 4B, $p < 0.05$). The modifications of Cyp2e1, Dhcr7, NR1, NR2B, CaMKIV and CREB1 were further validated by western-blot analysis shown in (Fig. 4C). In this study, c-Fos, Cyp2e1, NR1, NR2B, CaMKIV and CREB1 were increased by1.38-, 1.25-, 1.29-, 1.36-, 1.34- and 1.39-fold respectively, and Dhcr7 was decreased by 0.65-fold.

These results suggested that the repeated exposure to SnS_2 NFs in the high-dose group altered the expression of several genes involved in oxidative stress, metabolism, and signal transduction within brain tissues, supporting the fact that the SnS_2 NF-related neurotoxic phenotype was a physiological response and adapting mechanism for alien invasion.

Effects of SnS_2 NFs on apoptosis

The effects of SnS_2 NFs on apoptosis were evaluated by assay of the mRNA expression of genes regulating apoptosis. The apoptotic state can be checked by examining the expression of several genes involved in apoptosis. Four of the typical apoptotic genes Bax, Bcl-xl, Bcl-2 and Bim were evaluated by assay of the mRNA expression (Fig. 5). The expression of Bax in the 10 and 50 mg kg^{-1} groups was higher than in the control and 5 mg kg^{-1} groups ($P < 0.05$, Fig. 5A). The apoptotic cells were further identified in hippocampal neurons by TUNEL assay, which revealed only a few positive cells in control mice, indicating a basal level of apoptosis. The number of apoptotic cells

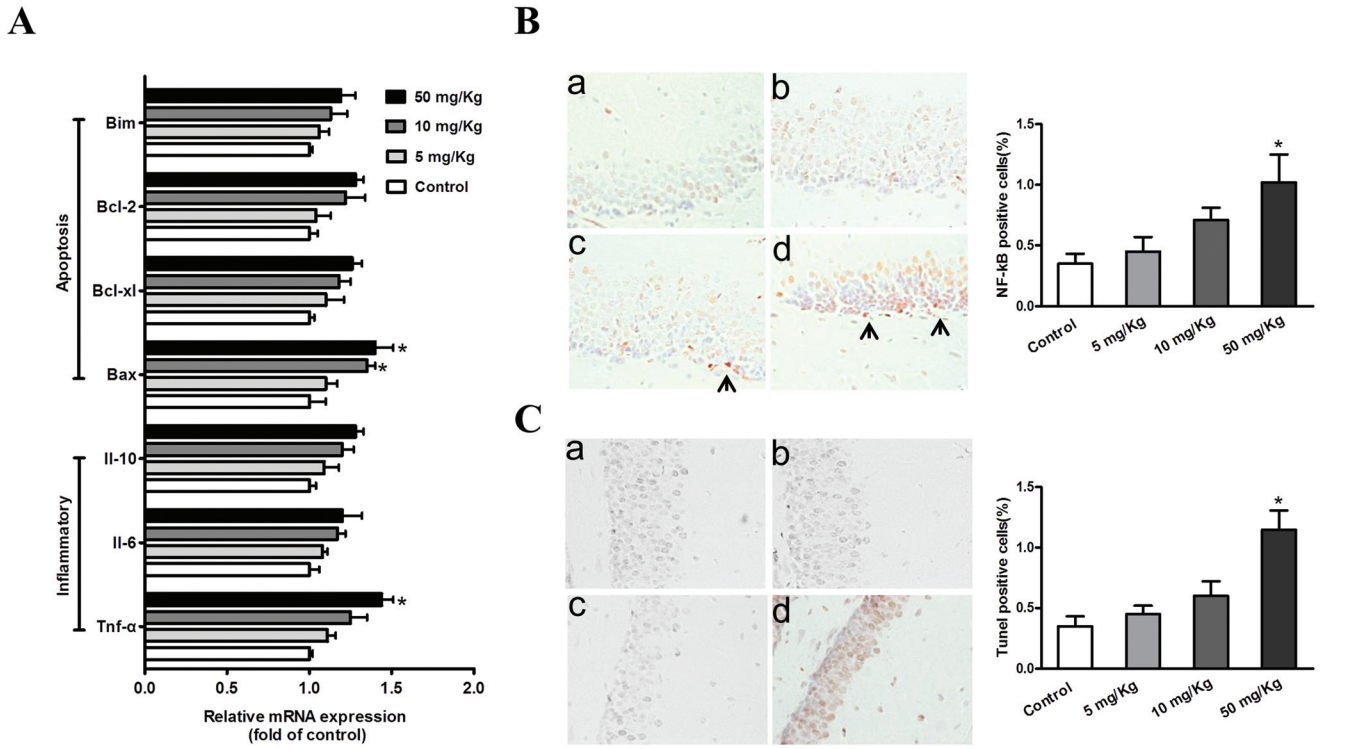

Fig. 5 Effect of SnS_2 NFs on brain inflammation and apoptosis. (A) Transcription levels of mRNAs encoding inflammatory factors and apoptotic genes in brain tissues of mice following SnS_2 NF exposure. Each bar represents the mean ± S.D. (n = 10). (B) Immunohistochemical staining of NF-κB (brown) in brain tissues of mice exposed to SnS_2 NFs *via* intragastric administration of 50 nm at ×400 magnification. (C) Hippocampal neuron cell apoptosis was detected by TUNEL staining at ×400 magnification (arrows).

was increased in hippocampal neurons of mice treated with 50 mg kg^{-1} SnS_2 NFs compared with the control (Fig. 5C).

Conclusions

Repeated intragastric administration of high-dose (50 mg kg^{-1}) SnS_2 NFs (50 nm) resulted in neurotoxicity and oxidative responses. Expression levels of genes related to oxidative stress, metabolism, and signal transduction were also modified in brain tissues from mice exposed to SnS_2 NFs, supporting the SnS_2 NF-dependent neurotoxic phenotype. Additionally, SnS_2 NF exposure led to an abnormal ultrastructure in the hippocampus of the treated mice. These data provided useful information for risk analysis and the regulation of nano-sized materials by administrative agencies.

Conflicts of interest

There are no conflicts of interest to declare.

Acknowledgements

This work was funded by the National Natural Science Foundation of China (No. 51572190).

References

1 H. Li, Q. Zhang, A. Pan, Y. Wang, B. Zou and H. J. Fan, Single-crystalline Cu4Bi4S9 nanoribbons: facile synthesis, growth mechanism, and surface photovoltaic properties, *Chem. Mater.*, 2011, **23**, 1299–1305.
2 Z. Wang, J. Liu, Y. Dai, W. Dong, S. Zhang and J. Chen, Dimethyl sulfide photocatalytic degradation in a Light-emitting-diode continuous reactor: kinetic and mechanistic study, *Ind. Eng. Chem. Res.*, 2011, **50**, 7977–7984.
3 A. Agarwal, P. D. Patel and D. Lakshminarayana, Single crystal growth of layered tin monoselenide semiconductor using a direct vapour transport technique, *J. Cryst. Growth*, 1994, **142**(142), 344–348.
4 G. Domingo, R. S. Itoga and C. R. Cannewurf, Fundamental optical absorption in SnS2 and SnSe2, *Phys. Rev.*, 1966, **143**, 536–541.
5 J. Zai, K. Wang, Y. Su, X. Qian and J. Chen, High stability and superior rate capability of three-dimensional hierarchical SnS2 microspheres as anode material in lithium ion batteries, *J. Power Sources*, 2011, **196**, 3650–3654.
6 M. S. Niasari, M. Bazarganipour, F. Davar and A. A. Fazlc, Simple routes to synthesis and characterization of nanosized tin telluride compounds, *Appl. Surf. Sci.*, 2010, **257**, 781–785.
7 W. D. Shi, L. H. Huo, H. S. Wang, H. J. Zhang, J. H. Yang and P. H. Wei, Hydrothermal growth and gas sensing prop-

erty of flower-shaped SnS2 nanostructures, *Nanotechnology*, 2006, **17**, 2918–2924.
8 M. S. Niasari, N. Mir and F. Davar, Synthesis, characterization and optical properties of tin oxide nanoclusters prepared from a novel precursor via thermal decomposition route, *Inorg. Chim. Acta*, 2010, **363**, 1719–1726.
9 J. Zeng, R. Li, S. Liu and L. Zhang, Fiber-like TiO2 nanomaterials with different crystallinity phases fabricated via a green pathway, *ACS Appl. Mater. Interfaces*, 2011, **3**, 2074–2079.
10 P. Bansal, D. Singh and D. Sud, Photocatalytic degradation of azo dye in aqueous TiO2 suspension: reaction pathway and identification of intermediates products by LC/MS, *Sep. Purif. Technol.*, 2010, **72**, 357–365.
11 D. Huang, Y. Miyamoto, T. Matsumoto, T. Tojo, T. Fan, J. Ding, Q. Guo and D. Zhang, Preparation and characterization of high-surface-area TiO2/activated carbon by low-temperature impregnation, *Sep. Purif. Technol.*, 2011, **78**, 9–15.
12 D. Wallach, S. Bar-Nun and I. Ohad, Assessment of SnS2 nanoparticles properties for photocatalytic and antibacterial applications, *Sol. Energy*, 2015, **117**(1), 187–191.
13 S. Amara, I. B. Slama, K. Omri, J. E. Ghoul, M. L. El, K. B. Rhouma, H. Abdelmelek and M. Sakly, Effects of nanoparticle zinc oxide on emotional behavior and trace element homeostasis in rat brain, *Toxicol. Ind. Health*, 2015, **31**(12), 1202–1209.
14 M. Afifi, S. Saddick and O. A. Zinada, Toxicity of silver nanoparticles on the brain of oreochromis niloticus and tilapia zillii, *Saudi J. Biol. Sci.*, 2016, **23**(6), 754–760.
15 A. Peters, B. Veronesi, L. Calderón-Garcidueñas, P. Gehr, L. C. Chen, M. Geiser, W. Reed, B. Rothen-Rutishauser, S. Schürch and H. Schulz, Translocation and potential neurological effects of fine and ultrafine particles a critical update, *Part. Fibre Toxicol.*, 2006, **3**, 13.
16 M. L. Block, X. Wu, Z. Pei, G. Li, T. Wang, L. Qin, B. Wilson, J. Yang, J. S. Hong and B. Veronesi, Nanometer size diesel exhaust particles are selectively toxic to dopaminergic neurons: the role of microglia, phagocytosis, and NADPH oxidase, *FASEB J.*, 2004, **18**, 1618–1620.
17 B. Song, J. Liu, X. Feng, L. Wei and L. Shao, A review on potential neurotoxicity of titanium dioxide nanoparticles, *Nanoscale Res. Lett.*, 2015, **10**(1), 342–359.
18 D. Bai, Q. Li, Y. Xiong, J. Zhao, L. Bai, P. Shen, L. Yuan and P. Wu, Effects of intraperitoneal injection of SnS2 flowers on mouse testicle, *Toxicol. Sci.*, 2017, **161**(2), 388–400.
19 D. Bai, Q. Li, Y. Xiong, C. Wang, P. Shen, L. Bai, L. Yuan and P. Wu, Hepatic, metabolic and toxicity evaluation of repeated oral administration of SnS2 nanoflowers in mice, *Toxicol. Sci.*, 2018, **164**(2), 501–511.
20 E. Zimcikova, J. Simko, I. Karesova, J. Kremlacek and J. Malakova, Behavioral effects of antiepileptic drugs in rats: are the effects on mood and behavior detectable in open-field test?, *Seizure*, 2017, **52**, 35–40.
21 Q. L. Zhang, M. Q. Li, J. W. Ji, F. P. Gao, R. Bai, C. Y. Chen, Z. W. Wang, C. Zhang and Q. Niu, In vivo toxicity of nano-alumina on mice neurobehavioral profiles and the potential mechanisms, *Int. J. Immunopathol. Pharmacol.*, 2011, **24**(1 Suppl), 23–29.
22 C. L. Bregman, R. R. Adler, D. G. Morton, K. S. Regan and B. L. Yano, Recommended tissue list for histopathologic examination in repeat-dose toxicity and carcinogenicity studies: A proposal of the society of toxicologic pathology (STP), *Toxicol. Pathol.*, 2003, **31**(2), 252–253.
23 C. P. Oliveira, F. P. Lopasso, F. R. Laurindo, R. M. Leitao and A. A. Laudanna, Protection against liver ischemia-reperfusion injury in rats by silymarin or verapamil, *Transplant. Proc.*, 2001, **33**, 3010–3014.
24 J. Nourooz-Zadeh, J. Tajaddini-Sarmadi and S. P. Wolff, Measurement of plasma hydroperoxide concentrations by the ferrous oxidationxylenol orange assay in conjunction with triphenylphosphine, *Anal. Biochem.*, 1994, **220**, 403–409.
25 S. Zhang, C. Jiang, H. Liu, Z. Guan, Q. Zeng and C. Zhang, Fluoride-elicited developmental testicular toxicity in rats: Roles of endoplasmic reticulum stress and inflammatory response, *Toxicol. Appl. Pharmacol.*, 2013, **271**(2), 206–215.
26 D. Ma, R. N. Zhang, Y. Wen, W. N. Yin, D. S. Bai, G. Y. Zheng, J. S. Li, B. Zheng and J. K. Wen, 1, 25(OH)2D3-induced interaction of vitamin D receptor with p50 subunit of NF-κB suppresses the interaction between KLF5 and p50, contributing to inhibition of LPS-induced macrophage proliferation, *Biochem. Biophys. Res. Commun.*, 2016, **482**(2), 366–374.
27 L. Ma, J. Liu, N. Li, J. Wang, Y. Duan, J. Yan, H. Liu, H. Wang and F. Hong, Oxidative stress in the brain of mice caused by translocated nanoparticulate TiO2 delivered to the abdominal cavity, *Biomaterials*, 2010, **31**(1), 99–105.
28 Z. Cheng, N. Li, J. Cheng, R. Hu, G. Gao, Y. Cui, X. Gong, L. Wang and F. Hong, Signal pathway of hippocampal apoptosis and cognitive impairment of mice caused by cerium chloride, *Environ. Toxicol.*, 2012, **27**(12), 707–718.
29 R. Walters, R. P. Kraig, I. Medintz, J. B. Delehanty, M. H. Stewart, K. Susumu, A. L. Huston, P. E. Dawson and G. Dawson, Nanoparticle targeting to neurons in a rat hippocampal slice culture model, *ASN Neuro*, 2012, **4**(6), 383–392.
30 K. Shrivas, T. Hayasaka, Y. Sugiura and M. Setou, Method for Simultaneous Imaging of Endogenous Low Molecular Weight Metabolites in Mouse Brain Using TiO2 Nanoparticles in Nanoparticle-Assisted Laser Desorption/Ionization-Imaging Mass Spectrometry, *Anal. Chem.*, 2011, **83**(19), 7283–7289.
31 Y. Ze, L. Zheng, X. Zhao, S. Gui, X. Sang, J. Su, N. Guan, L. Zhu, L. Sheng, R. Hu, J. Cheng, Z. Cheng, Q. Sun, L. Wang and F. Hong, Molecular mechanism of titanium dioxide nanoparticles-induced oxidative injury in the brain of mice, *Chemosphere*, 2013, **92**(9), 1183–1189.
32 J. K. Folkmann, L. Risom, N. R. Jacobsen, H. Wallin, S. Loft and P. Møller, Oxidatively damaged DNA in rats exposed by oral gavage to C60 fullerenes and single-walled carbon nanotubes, *Environ. Health Perspect.*, 2009, **117**(5), 703–708.

33 H. L. Su, C. C. Chou, D. J. Hung, S. H. Lin, I. C. Pao and J. H. Lin, The disruption of bacterial membrane integrity through ROS generation induced by nanohybrids of silver and clay, *Biomaterials*, 2009, **30**(30), 5979–5987.

34 E. J. Park, J. Yoon, K. Choi, J. Yi and K. Park, Induction of chronic inflammation in mice treated with titanium dioxide nanoparticles by intratracheal instillation, *Toxicology*, 2009, **260**(1–3), 37–46.

35 C. Carlson, S. M. Hussain, A. M. Schrand, L. K. Braydich-Stolle, K. L. Hess, R. L. Jones and J. J. Schlager, Unique Cellular Interaction of Silver Nanoparticles: Size-Dependent Generation of Reactive Oxygen Species, *J. Phys. Chem. B*, 2008, **112**(43), 13608–13619.

36 A. Liu, N. Tanaka, L. Sun, B. Guo, J. H. Kim, K. W. Krausz, Z. Fang, C. Jiang, J. Yang and F. J. Gonzalez, Saikosaponin d protects against acetaminophen-inducedhepatotoxicity by inhibiting NF-kappaB and STAT3 signaling, *Chem.-Biol. Interact.*, 2014, **223**, 80–86.

37 Z. Tan, A. Liu, M. Luo, X. Yin, D. Song, M. Dai, P. Li, Z. Chu, Z. Zou, M. Ma, B. Guo and B. Chen, Geniposide inhibits alpha-naphthylisothiocyanate-Inducedintrahepatic cholestasis: the downregulation of STAT3 and NF-κB signaling plays an important role, *Am. J. Chin. Med.*, 2016, **44**, 721–736.

38 V. Elzakke M, R. D. Fevurly, T. Breindel and R. L. Spencer, Environmental novelty is associated with a selective increase in Fos expression in the output elements of the hippocampal formation and the perirhinal cortex, *Learn. Mem.*, 2008, **15**, 899–908.

39 M. Dragunow and R. Faull, The use of c-Fos as a metabolic marker in neuronal pathway tracing, *J. Neurosci. Methods*, 1989, **29**, 261–265.

40 H. E. Day, E. M. Kryskow, T. J. Nyhuis, L. Herlihy and S. Campeau, Conditioned Fear Inhibits c-fos mRNA Expression in the Central Extended Amygdala, *Brain Res.*, 2008, **1229**, 137–146.

41 Y. Ze, R. Hu, X. Wang, X. Sang, X. Ze, B. Li, J. Su, Y. Wang, N. Guan, X. Zhao, S. Gui, L. Zhu, Z. Cheng, J. Cheng, L. Sheng, Q. Sun, L. Wang and F. Hong, Neurotoxicity and gene-expressed profile in brain-injured mice caused by exposure to titanium dioxide nanoparticles, *J. Biomed. Mater. Res., Part A*, 2014, **102**(2), 470–478.

42 X. Ze, M. Su, X. Zhao, H. Jiang, J. Hong, X. Yu, D. Liu, B. Xu, L. Sheng, Q. Zhou, J. Zhou, J. Cui, K. Li, L. Wang, Y. Ze and F. Hong, TiO2 nanoparticle-induced neurotoxicity may be involved in dysfunction of glutamate metabolism and its receptor expression in mice, *Environ. Toxicol.*, 2016, **31**(6), 655–662.

43 M. Su, L. Sheng, X. Zhao, L. Wang, X. H. Yu, J. Hong, B. Q. Xu, D. Liu, H. Jiang, X. Ze, Y. T. Zhu, Y. Long, J. L. Zhou, J. W. Cui, K. Li, Y. G. Ze and F. Hong, Involvement of neurotrophins and related signaling genes in TiO2 nanoparticle–induced inflammation in the hippocampus of mouse, *Toxicol. Res.*, 2015, **4**(2), 344–350.

44 M. F. Rahman, J. Wang, T. A. Patterson, U. T. Saini, B. L. Robinson, G. D. Newport, R. C. Murdock, J. J. Schlager, S. M. Hussain and S. F. Ali, Expression of genes related to oxidative stress in the mouse brain after exposure to silver-25 nanoparticles, *Toxicol. Lett.*, 2009, **187**(1), 15–21.

45 Y. Lu and A. I. Cederbaum, CYP2E1 and oxidative liver injury by alcohol, *Free Radical Biol. Med.*, 2008, **44**(5), 723–738.

46 H. R. Waterham and R. J. Wanders, Biochemical and genetic aspects of 7-dehydro-cholesterol reductase and Smith–Lemli–Opitz syndrome, *Biochim. Biophys. Acta*, 2001, **1529**, 340–356.

47 D. M. Bannerman, M. A. Good, S. P. Butcher, M. Ramsay and R. G. Morris, Distinct components of spatial learning revealed by prior training and NMDA receptor blockade, *Nature*, 1995, **378**, 182–186.

48 J. Z. Tsien, P. T. Huerta and S. Tonegawa, The essential role of hippocampal CA1 NMDA receptor-dependent synaptic plasticity in spatial memory, *Cell*, 1996, **87**, 1327–1338.